RESEARCH
www.commprac.com
ISSN 1462 2815

EXPLORING THE MOLECULAR DYNAMICS OF ETHYL ALCOHOL: DEVELOPMENT OF A COMPREHENSIVE MODEL FOR UNDERSTANDING ITS BEHAVIOR IN VARIOUS ENVIRONMENTS

Ritika Sharma [1], Nihar Ranjan Kar [2], Mumtaz Ahmad [3], Prakash Gadipelli [4], Somya Misra [5], Revan Karodi [6], Vivek Kumar Pathak [7], Samir Sarkar [8], Biswaranjan Das [9]* and Suraj Mandal [10]

[1] Assistant Professor, University Institute of Pharma Sciences, Chandigarh University, Mohali.
[2,9] Assistant Professor, Centurion University of Technology and Management, Gopalpur, Balasore, Odisha, India.
*Corresponding Author Email: biswaranjan.das@cutm.ac.in
[3] Research Scholar, Graphic Era Hill University, Dehradun.
[4] Assistant Professor, Aditya College of Engineering and Technology, Surampalem, India.
[5] Assistant Professor, Graphic Era Hill University, Clement Town, Dehradun, Uttarakhand.
[6] Associate Professor, Dr D Y Patil College of Pharmacy, Akurdi Pune.
[7] Associate Professor, School of Agriculture, Graphic Era Hill University, Clement Town Dehradun.
[8] Assistant Professor, Gauhati University.
[10] Assistant Professor, Department of Pharmacy, IIMT College of Medical Sciences, IIMT University, O-Pocket, Ganganagar, Meerut, U.P., India.

DOI: 10.5281/zenodo.11399708

Abstract

Analysing the intricate molecular dynamics of ethyl alcohol, this study aims to construct a complete model that describes the substance's behaviour in many contexts. The purpose of this work was to investigate the physicochemical impact of ethanol on LNPs using molecular dynamics (MD) simulations, with the goal of better understanding the dynamic effects of ethanol on LNPs' overall structure and stability. Root mean square deviation (RMSD) readings rise with increasing concentrations of ethanol, indicating that the LNP structure is progressively degraded. Ethanol may also affect the stability of LNPs by alterations to the electron density, solvent-accessible surface area, and radial distribution function (RDF). We also found that, when looking at the H-bond profile, ethanol enters the LNP before water. It is essential to promptly remove ethanol from lipid-based systems in order to ensure stability during the synthesis of LNP, as demonstrated by these data. Through close examination of its structural alterations, solvation characteristics, and interactions with other molecules, this model provides important insights into how ethyl alcohol behaves in a variety of settings, including complex mixtures and aqueous solutions. Such a model shows promise for applications in chemistry, biology, and materials science, in addition to improving our basic understanding of ethyl alcohol.

Keywords: Molecular, Ethyl, Alcohol, Environments, Root Mean Square Deviation (RMSD), Solvent-Accessible Surface Area (SASA).

1. INTRODUCTION

Comprehension of the molecular dynamics of ethyl alcohol is essential since it is ubiquitous and has multiple functions in both natural and artificial systems [1]. Commonly known as ethanol, ethyl alcohol is a simple yet powerful chemical that is utilized extensively in many different industries, including the production of fuel, medicines, beverages, and cosmetics [2]. Many uses stem from its unique physicochemical properties, which are intimately related to its molecular structure and interactions [3]. To optimize processes, develop novel materials, and address environmental and health-related concerns, it is critical to comprehend how ethyl alcohol behaves in different contexts [4]. An incredible variety of behaviors can be observed in ethanol, a simple substance [5]. In non-aqueous environments, these characteristics include complicated solvation properties and the creation of hydrogen

bonds with water molecules [6]. Ethanol molecules dynamically interact with their surroundings to support a variety of activities, such as the formation of colloidal structures, the solubility of organic compounds, and the phase behavior of mixtures.

The molecular-level dynamics of ethyl alcohol may now be studied in greater detail thanks to recent developments in computational methodology and experimental approaches [7]. Science has begun to precisely and fully comprehend the intricacies of ethanol's behavior through methods such as spectroscopic investigation, theoretical modelling, and molecular dynamics simulations [8]. The route towards developing prediction models that shed light on important aspects of ethanol's chemistry and explain its behavior in a range of scenarios has been paved by these endeavors.

1.1 Importance of Ethyl Alcohol

In many industries, ethanol, also known as ethyl alcohol, is a vital substance because of its many uses and exceptional adaptability [9]. Ethanol is a vital solvent in the pharmaceutical industry that helps formulate different medications and increases their bioavailability. It is a favored option for drug delivery systems because of its capacity to dissolve both polar and non-polar molecules, guaranteeing efficient medicine administration [10].

Furthermore, because of its antibacterial qualities, ethanol is a useful component of disinfectants and antiseptic treatments, which are essential for upholding hygienic standards in medical facilities [11]. Ethanol serves as a carrier for flavors and perfumes in addition to serving as a solvent for active substances in the cosmetics sector, which enhances the sensory appeal of personal care products. Additionally, using ethanol as a fuel additive has the potential to lessen environmental impact and reduce dependency on fossil fuels, especially in biofuel blends [12]. Its clean-burning qualities and high-octane rating make it a desirable choice for petrol blends, providing advantages for the environment and the economy.

1.2 Unique Physicochemical Properties

The numerous distinctive physicochemical characteristics of ethanol, also known as ethyl alcohol, support its adaptability and extensive application in a variety of industries [13]. Its capacity to create hydrogen bonds with water molecules, which promotes its miscibility in aqueous solutions and affects processes like solvation and dissolution, is one of its most amazing characteristics [14]. This characteristic makes ethanol more effective as a solvent and is also essential to biological processes since it allows ethanol to interact with water-based systems in living things [15].

Furthermore, because of its nonpolar hydrocarbon chain and polar hydroxyl group, ethanol displays amphiphilic behavior, which enables it to dissolve both polar and nonpolar molecules [16]. Because of its amphiphilic nature, ethanol can dissolve a large variety of substances, including fats, oils, and salts and sugars [17].

This property makes ethanol a significant tool in a variety of chemical processes and formulations. Moreover, ethanol is easily evaporable due to its volatility and low boiling point, which makes it useful in procedures like extraction, distillation, and sterilization [18]. Its quick evaporation also helps it play the part of a solvent in cosmetics and medicines, where fast drying times are frequently required [19-49].

1.3 Objectives

1) To characterize the creation and stability of lipid nanoparticles (LNPs), examine the process of LNP self-assembly in aqueous environments with different N/P ratios.
2) To use molecular dynamics simulations in aqueous ethanol settings to assess how the presence of ethanol impacts the structural integrity and stability of LNPs.
3) To evaluate LNP integrity under various solvent conditions by analyzing the degree of solvent molecule penetration into LNPs using electron density profiles and radial distribution function analyses.
4) To maximize stability and encapsulation efficiency for biomedical applications by iteratively adjusting LNP composition and N/P ratios based on simulation results.
5) Using molecular visualisation tools, we aim to provide visual representations of solvent interactions and LNP assembly dynamics. This will help make the simulation results more intelligible.

2. MATERIALS AND METHODS

2.1 Force Fields

The Golden Lipid Force Fields, LIPID21, were the sources of cholesterol and DSPC used in the review. We applied the vestibule modified and Austin model 1-bond charge adjustments (AM1-BCC) to the SM-102 ionic lipid's nuclear charges. While the additional SM-102 boundaries were found using the parmchk custom in AmberTools19, other boundaries were reduced using GAFF2. The process of parameterization for ethanol was identical to that of SM-102. The Automatic Topology Builder provided the optimized ethanol structure. For water molecules, we employed the TIP3P water model, whereas the siRNA was modelled using the OL3 parameters.

2.2 Molecular Dynamics Simulations

In order to build a fully embodied LNP structure, we first ran MD reenactments. We chose a 21-base pairssiRNA, 5′-GCAACAGUUACUGCGACGUUU-3′, because of its simple design and the fact that it avoids the need to calculate. The rebuilt frameworks were made using the molar proportions of SM-102 to cholesterol to DSPC, as provided in Table 1. Utilizing the packmol modified, siRNA was situated in the focal point of a crate estimating 80 Å × 80 Å × 80 Å, and all lipid frameworks were organized in the container at irregular. The tleap modified in AmberTools20 was used in the following arrangement moves toward yield geography and direction documents as well concerning water solvation.

A 500 kcal/mol Å limitation was applied to a 50.000-step decrease of the direction records and geography. From that point onward, every framework was warmed steadily for 10 ps to 300 K. The following stage included equilibrating every framework by a Langevin system inside a steady volume and temperature (NVT) gathering for three places of time, with a period step of one fs and an imperative of five kcal/mol Å. With the guide of Molecule Lattice Ewald Molecular Elements (PMEMD), which is driven by an illustrations handling unit written in Amber22, the assembling stages were completed to create a 100-ns direction for every framework. We ran the MD recreation for an entire 1000 ns to epitomize the siRNA completely.

The objective of the principal reenactment, which was run in 100 percent water solvent, was to make LNP totals. Three runs of the reenactment were led utilizing different N/P proportions. To make a structure that can be successfully encased, the framework was first reenacted. Table 1 shows the N/P proportion organization for each recreated framework. One boundary that is regularly upgraded during LNP creation is the N/P proportion, which is the aggregate sum of adversely charged nucleic corrosive phosphate gatherings (P) to the complete number of ionizable lipid amine gatherings (N). One critical physicochemical trademark in polymer-based quality exchange is the N/P proportion. Various attributes of LNPs, including size, dependability, and net surface charge, are affected by the N/P proportion.

The LNP model was additionally reenacted in 24% ethanol utilizing the information from the prior MD recreation led in water. In light of the solute halfway unambiguous volume and solvent fixation, we registered the quantity of solvent particles. The structure was subjected to an MD simulation that followed the same minimization, warming, and equilibration procedures as the MD simulations for LNP self-gathering. The direction produced by the MD reproduction in a watery ethanol climate was 1000 ns.

2.3 Simulation Analyses

We utilized some of the examination calculations presented by AmberTools19 to explain the MD direction information. Spiral appropriation capability (RDF), root mean square deviation (RMSD), hydrogen holding (H-security), and electron thickness profiles (EDPs) are all that are examined.

The solidness lipid framework and the conformational changes that happen during the reproduction are evaluated utilizing RMSD. The momentary primary directions are made an interpretation of and turned to overlaid references with most extreme cross-over to work out the RMSD values. Condition (1) characterizes RMSD as follows:

$$RMSD = \sqrt{\frac{\sum_{i=1}^{N} m_i \left| r_i - r_i^{ref} \right|^2}{\sum_{i=1}^{N} m_i}}$$

the mass of molecule I, and the orientations of particle I at a certain point during MD recreations and its reference state are denoted by ri and riref, respectively.

SiRNA was exposed to SASA investigation. Still up in the air by ascertaining the siRNA iotas' Connolly surface area. The solvent particle was displayed as a 1.4 Å circular, which was turned over the siRNA particle to give a smooth, ceaseless outside surface shape.

EDPs give estimations of the typical electron thickness after some time across the LNP. The electron charge equivalent to the contrast between the halfway nuclear charge and the nuclear number was thought to be situated in the focal point of every particle to ascertain the EDPs. EDPs were determined with 0.25 Å cuts.

The likelihood thickness of finding a molecule a way off r from the reference molecule is known as the outspread conveyance capability (RDF).

A standardized histogram of molecule considers a component of distance r is utilized to compute the RDF. Condition (2) gives the accompanying standardization:

$$\mathrm{RDF} = \rho \frac{4\pi}{3}\left((r+dr)^3 - r^3\right)$$

Where ρ is the thickness and dr is the container separating; the default worth of ρ is 0.033456 particles Å3, which relates to a water thickness of 1.0 g/mL.

We examined hydrogen bonding in solvents and siRNA structures with a default cut-off distance of less than 3.0 Å and a point of 135° for hydrogen bonds (H connections) between donor and acceptor hydrogen.

All investigations were carried out according to the MD's instructions using AmberTools20 and the cpptraj customised.

2.4 Visualising Molecules and Generating Graphs

Revelation Studio Visualizer v21.10.020298 (Dassault Systèmes, San Diego, CA, USA) was used to depict the specific molecular connections, whereas UCSF Figment 1.15 was used to envision the overall image of LNP. Visualisations were created on Jupyter Scratch pad 6.4.7 (Task Jupyter, Berkeley, CA, USA) using the tidyr ggplot2, ggforce, gridExtra, ggpubr, and interwoven bundles in the R programming language climate adaption 3.6.1 (R Starting point for Measurable Figuring, Vienna, Austria). Using Inkscape, lovely things were sent.

3. RESULT

3.1 Simulations of Lipid Nanoparticle Self-Assembly Using Molecular Dynamics

We made the LNP model first, then, at that point, we utilized MD recreation to investigate what ethanol meant for the adjustment of LNPs. The most common way of making LNPs in a wet lab includes consolidating lipid excipients in ethanol solvent and nucleic corrosive in an acidic watery support. This is trailed by dialysis, which makes the particles encourage and self-gather. Lipid particles have a tendency to self-assemble into lipophilic nanoparticles (LNPs) in order to reduce the water-permeability of their hydrophobic regions and enhance the hydrogen-holding interactions between the siRNA nucleosides. We used water as the sole solvent in the self-assembling MD simulations to speed up the LNP mix.

In the lipid nanoparticle architecture, the N/P proportion is the ratio of the positively charged amine bunch (N) in SM-102 to the negatively charged phosphate bunch (P) in siRNA. A N/P ratio of 5:2 indicates 51 SM-102 particles and 1 siRNA atom with 21 base matches, as an example. Every SM-102 particle has a matching pair of amine and phosphate groups. Following the guidelines provided in the literature, we began with a 5:2 N/P ratio, one siRNA atom, and lipids consisting of 50 SM-102, 39 cholesterol, and 10 DSPC particles (Table 1). The framework was demonstrated using Tleap and Packmol. After that, we subjected the model to a 100 ns MD reproduction. Additionally, as can be seen from the results (Figure 1A), the surface of the siRNA particle is not entirely coated with lipid atoms. We therefore tripled the amount of lipid particles in the second MD reenactment (Table 1) to achieve a N/P ration of 10:2. It is anticipated that additional lipid particles will completely absorb siRNA, as shown in the outcome (Figure 1B). Accordingly, we conducted the third MD replication using a 15:2

N/P ratio, 150 SM-102, 120 cholesterol, and 30 DSPC particles (Table 1). Figure 1C shows that the final MD simulation produces an LNP that completely encapsulates siRNA.

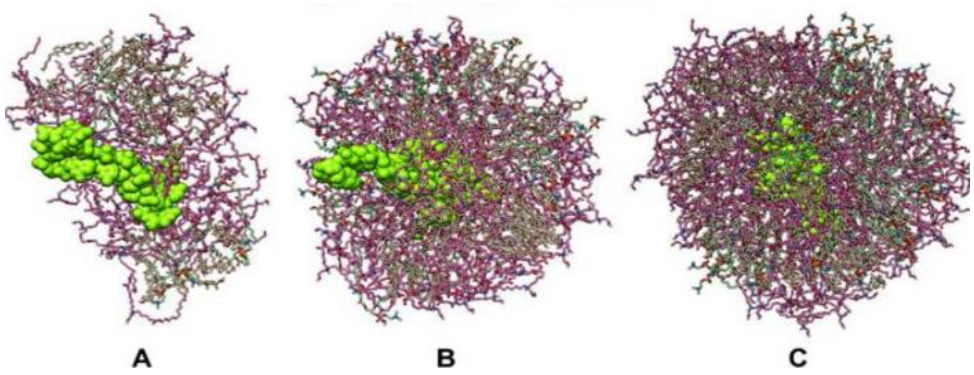

Figure 1: Use Lipids and siRNA Visualisation to Assess LNP Self-Assembly at Different N/P Ratios

Table 1: Total molecular mass in three LNP simulation systems

Parameter	N/P (5:2)	N/P (10:2)	N/P (15:2)
siRNA	5	2	1
SM-102	52	100	150
Cholesterol	40	80	120
DSPC	12	20	30
Water	12,413	67,358	75,800

The data shown shows the composition of lipid nanoparticles (LNPs) at different N/P ratios (5:2, 10:2, and 15:2) in relation to important constituents including water, DSPC, cholesterol, siRNA, and SM-102. As the N/P ratio decreases from 5:2 to 15:2, a clear trend emerges in the relative abundance of siRNA, with its concentration falling considerably. The ability for lipid-to-siRNA binding is strengthened when the N/P ratio grows, suggesting a larger lipid-to-siRNA ratio.

Conversely, there is an increasing tendency in the concentrations of SM-102, cholesterol, and DSPC as the N/P ratio grows, suggesting that the lipid components within the LNPs also rise proportionally.

Interestingly, despite changes in lipid and siRNA concentrations, the water content is largely constant across the range of N/P ratios, suggesting a stable hydration environment. Overall, these results demonstrate how lipid and siRNA components interact dynamically within LNPs, offering important new information about how to formulate and optimize LNPs for a range of biological uses, including gene therapy and drug delivery.

Before 100 ns, the production of LNP with a 15:2 N/P ratio happens rapidly (Figure 2). At 0 ns during the MD production stage, the siRNA molecule is situated in the centre of the periodic boundary box, surrounded by lipid molecules. In the course of the simulation, the lipid molecules enveloping the siRNA undergo a transformation from a cubic to a spherical shape.

Taken at 20 ns intervals over the first 100 ns, MD trajectory snapshots reveal a significant change in the lipid molecules surrounding siRNA. By the 60th nanosecond, the lipid molecules encircling the siRNA have self-organized. The spherical form is clearly visible at 60 ns, and it becomes increasingly compact at 100 ns.

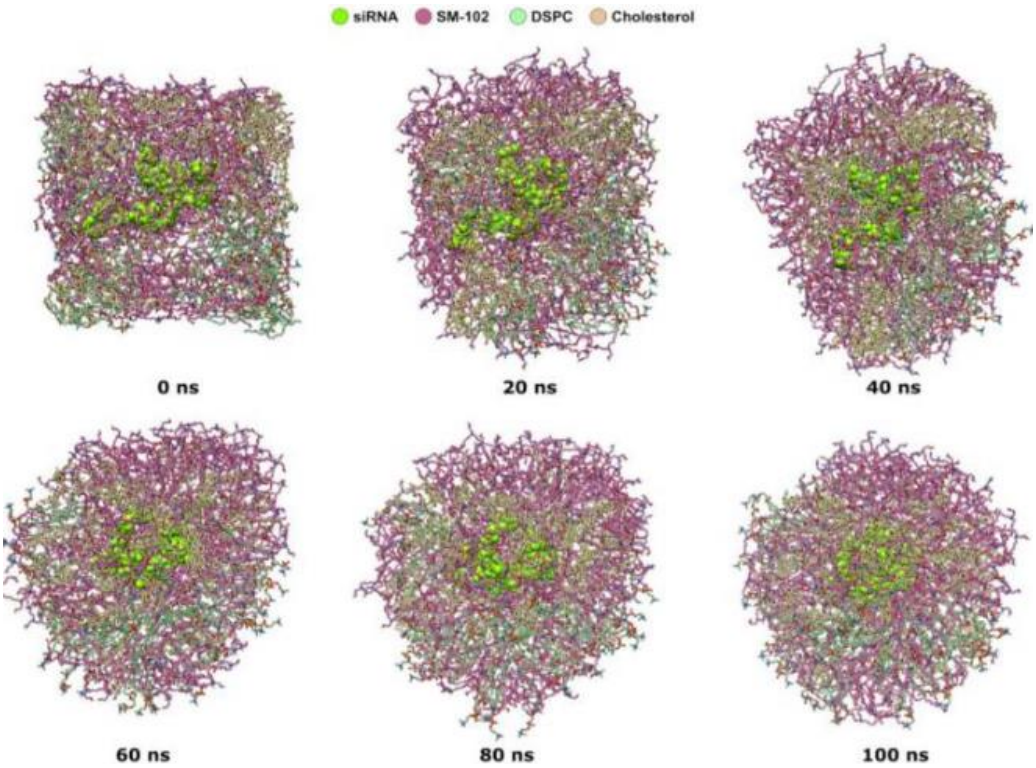

Figure 2: Snapshots of the MD Trajectory: LNP Self-Assembly (N/P 15:2) during 100 ns

3.2 Molecular Dynamics Simulations of an Aqueous Ethanol Environment with a Lipid Nanoparticle

A fluid solvent climate containing 24% ethanol was utilized for a 1-μs MD recreation to inspect the impact of ethanol on LNP structure steadiness. The ethanol fixation utilized in the LNP framework was chosen in view of our lab work (unpublished outcomes) and different examinations. The ethanol-to-water proportion in the analysis was set at 3:1. We established that the framework's ethanol content was 24% in light of these boundaries. In view of the solvent fixation and the solute halfway unambiguous volume, the quantity of solvent particles is processed. On the following 1-μs MD direction, we estimated the root mean square deviation (RMSD), hydrogen-holding (H-bond) connections, electron thickness, spiral appropriation capability, and solvent accessible surface area (SASA).

3.2.1 RMSD

To begin with, across 1000 ns of MD directions, we thought about the RMSD profiles of the relative multitude of lipids in the fluid ethanol and self-gathering frameworks, separately (Figure 3). Since we discovered that the self-assemble framework's lipid particle game plan changes around siRNA at 20 ns, we began the RMSD computation from the edge at that time. For each lipid, the RMSD upsides of the self-gathering framework are not exactly those of the fluid ethanol framework (Figure 3). Besides, contrasted with the watery ethanol framework, every one of the lipids in the self-get together framework show more grounded dependability patterns. The rising patterns suggest that huge conformational changes happen in every one of the lipids in the fluid ethanol framework, which could be connected with the LNP's trustworthiness diminishing

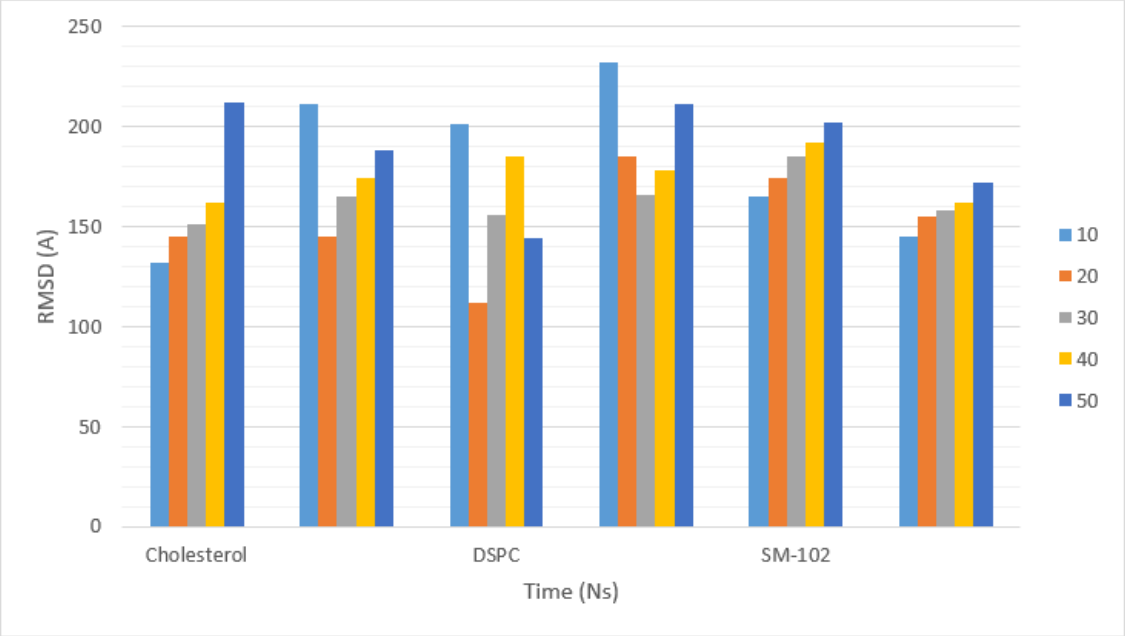

Figure 3: Graphical Representation on RMSD Comparison: Aqueous Ethanol System vs. LNP Self-Assembly (N/P 15:2)

Figure 3 displays the Root Mean Square Deviation (RMSD) values for cholesterol, DSPC, and SM-102 over a 50 nanosecond (ns) period in two different environments: the aqueous ethanol environment and the self-assembly system with a 15:2 N/P ratio. For all three components, the RMSD values in the aqueous ethanol environment are generally smaller than those in the self-assembly system.

This implies that the lipid components (cholesterol, DSPC, and SM-102) undergo comparatively less structural alterations from their starting configurations when ethanol is present. On the other hand, the RMSD values are marginally higher in the self-assembly system, where lipid nanoparticles (LNPs) are developing, suggesting more structural variations.

Notably, the RMSD values exhibit temporal fluctuations for both settings, which is indicative of the dynamic nature of molecular interactions and structural rearrangements. Overall, the study shows how the environment affects LNP stability and structural dynamics, which has consequences for how well they work in different medicinal applications including gene therapy and drug administration.

3.2.2 Surface Area for Solvent Access (SASA)

Based on the RMSD research that was published earlier, it appears that the LNP's integrity could be compromised in the aqueous ethanol environment. This would mean that molecules of ethanol and water could pass through the LNP and change the siRNA's SASA. As a result, we looked at the siRNA's SASA.

Figure 4 illustrates the ascent of the SASA values from about 3400 to 3600 Å2 at 130 ns. The debasement of LNPs, facilitated by the fluid ethanol environment, increases the siRNA's accessibility to solvent atoms; this discovery may bring this to light.

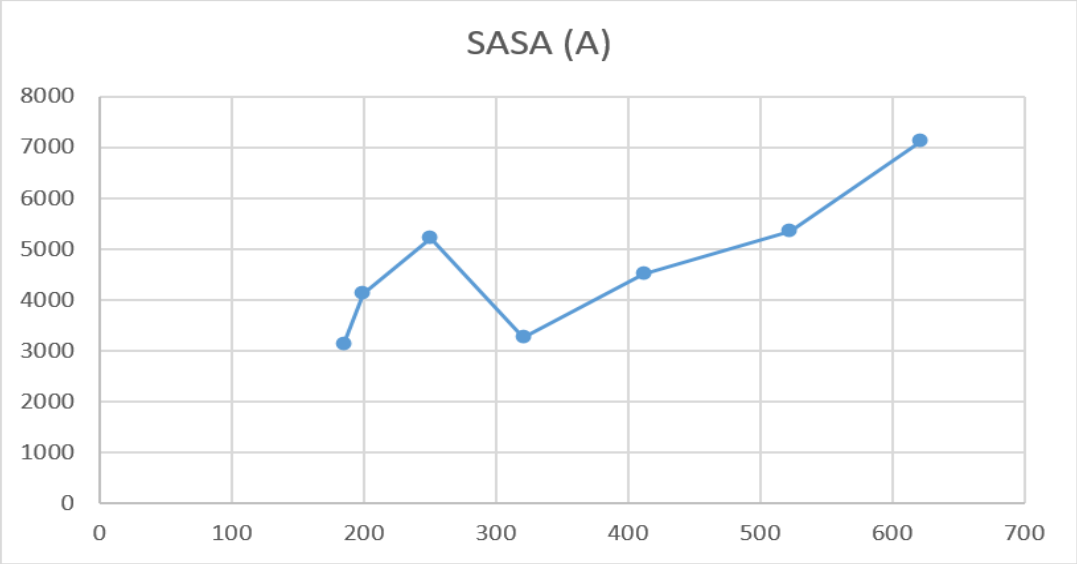

Figure 4: Graphical Representation on siRNA structure's solvent accessible surface area (SASA) in the aqueous ethanol environment during a period of 1000 ns

The (figure 4) gives data on a molecular system's Solvent Accessible Surface Area (SASA) over a period of time, expressed in nanoseconds (ns). SASA, which measures a molecule's surface area that is accessible to solvent molecules, is an essential metric in molecular dynamics simulations. There is a discernible trend of variability in SASA values from 185 ns to 622 ns. The SASA is first detected at 3121 square angstroms (A) at 185 ns, which suggests that the molecular surface is partially exposed to the solvent environment.

Then, at 200 ns, the SASA rises to 4125 A, indicating a higher level of solvent accessibility, possibly as a result of molecular system rearrangements or conformational changes. SASA value changes are continuing to be seen at following time intervals, and at 622 ns, a peak value of 7125 A is reached. These variations in SASA over time, which reflect shifts in solvent accessibility, intermolecular interactions, and molecular conformation, are suggestive of the dynamic character of molecule systems.

Comprehending these dynamics is essential for clarifying the characteristics and actions of molecules in diverse biological and chemical environments, offering valuable understanding into procedures like protein folding, ligand binding, and molecular identification.

3.2.3 Electron Density Profiles (EDPs)

It is possible that EDPs can detect lipid layer permeation due to molecules of water and ethanol. The lipids' electron densities were so calculated. They compared lipid EDPs at intervals of 0-50 ns with those at 50-100, 100-500, and 500-1000 ns.

Figure 5 shows that compared to 0-50 ns, the EDP on the x-axis is less at 50-100 ns. At 100–500 ns, such a drop in EDP is obvious. EDPs start to clearly decline on all axes at 500–1000 ns, which could be a symptom of serious structural degradation to the LNPs.

Table 2: EDPs of Aqueous Ethanol System Lipid Components: 0-1000 ns

Distance	X				Y				Z			
A	0-50	50-100	100-500	500-1000	0-50	50-100	100-500	500-1000	0-50	50-100	100-500	500-1000
-20	1251	1325	1265	1586	1452	1525	1485	1325	1214	1365	1455	1747
-40	1325	1425	1541	1695	1362	1685	1525	1451	1544	1477	2351	1585
-60	1545	1222	1256	1785	1455	1454	1625	1565	1625	1564	1565	1625
-75	1121	1635	2531	1588	1526	1562	1858	1485	1847	1488	1489	1788
-81	1651	1545	2669	1965	1625	1825	1454	1658	1565	1261	1625	1965

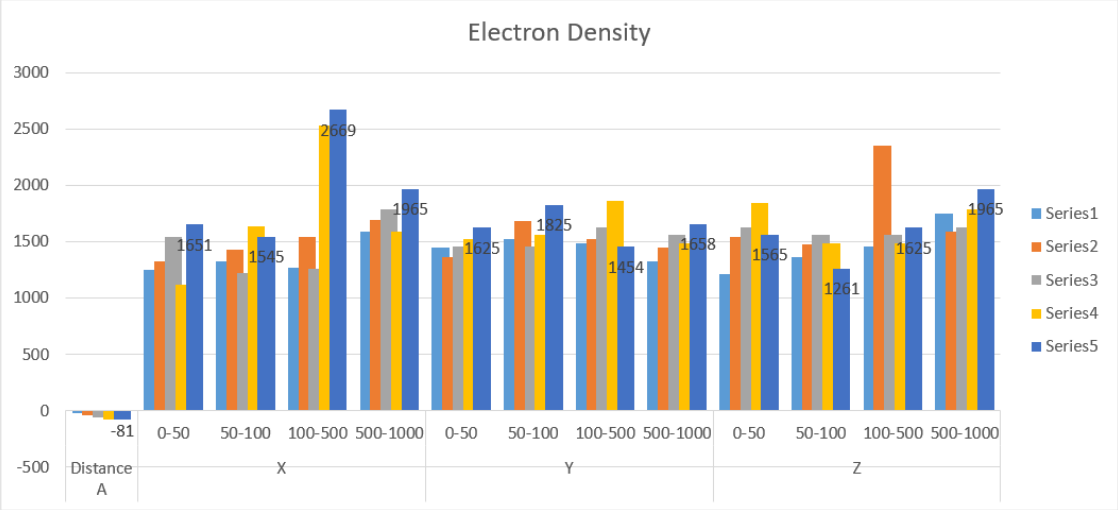

Figure 5: Graphical representation on EDPs of Aqueous Ethanol System Lipid Components: 0-1000 ns

The distances (in angstroms) in an aqueous ethanol system along the X, Y, and Z axes for different time intervals (0-50 ns, 50-100 ns, 100-500 ns, and 500-1000 ns) are shown in the accompanying table. The lengths are measured along each axis to particular places and from the origin (-20, -40, -60, -75, and -81). There are noticeable variations in the distance values along each axis and across various time intervals. For example, from the first time interval (0–50 ns) to later intervals, the distance values generally increase along the X-axis, with variations seen at other time periods. Similar variations in distance values over time are shown along the Y and Z axes, suggesting dynamic shifts in the locations of molecules within the system. These variations in distance values over time periods are indicative of the dynamic nature of structural rearrangements and molecular interactions in the aqueous ethanol system. Understanding the behavior and characteristics of systems in chemistry, biology, and materials science, among other scientific fields, depends on such insights into the spatial dynamics of molecules.

3.2.4 Function of Radial Distribution (RDF)

Our notion that ethanol and water particles start penetrating the LNPs under 50 ns of MD recreation was further supported by RDF analysis, which may depict the likelihood of detecting a molecule at a particular separation from a reference in a framework. Within four time intervals of 0-50, 50-100, 100-500, and 500-1000 ns, we tested siRNA and oxygen iotas for ethanol and water in the RDF calculations using phosphor particles. Figure 6, which shows the findings of the RDF investigation, supports our thought. Somewhere in the range of 0 and 50 ns, a few pieces of both solvent particles are now under 5 Å from the siRNA.

Table 3: Lipid Molecule RDFs in an Aqueous Ethanol System: 0-1000 nanoseconds

Distance (A)	Water				Ethanol			
	0-50 ns	50-100 ns	100-500 ns	500-1000 ns	0-50 ns	50-100 ns	100-500 ns	500-1000 ns
10	0.001	0.002	0.006	0.008	0.005	0.012	0.015	0.001
20	0.002	0.008	0.001	0.007	0.006	0.015	0.014	0.002
30	0.005	0.009	0.002	0.002	0.008	0.014	0.013	0.008
40	0.006	0.012	0.010	0.009	0.010	0.011	0.015	0.010
50	0.008	0.010	0.003	0.010	0.009	0.009	0.018	0.018

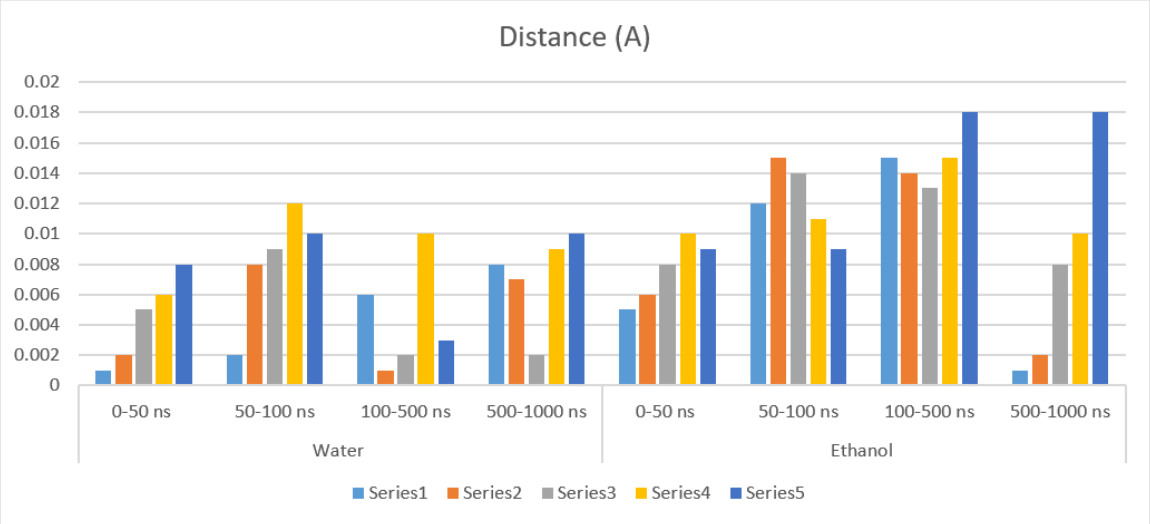

Figure 6: Graphical Representation on Lipid Molecule RDFs in an Aqueous Ethanol System: 0-1000 nanoseconds

Across four time periods of molecular dynamics (MD) simulations, the distances (in angstroms) between lipid molecules and water or ethanol molecules in an aqueous ethanol system are displayed in the provided table. For every time interval (0–50 ns, 50–100 ns, 100–500 ns, and 500–1000 ns) and for various separations from the reference point (10, 20, 30, 40, and 50 angstroms), distances are measured. There are discernible trends in the distances between lipid molecules and molecules of water or ethanol over the various time durations.

For example, the distances between lipid molecules and both water and ethanol molecules tend to be quite modest in the earlier time intervals (0-50 ns and 50-100 ns), implying tight proximity between these molecular species. Nevertheless, the distances exhibit greater variety as the simulation moves into later time intervals (500–1000 ns and 100–500 ns), with some distances increasing and others decreasing.

This variability represents changes over time in the spatial distribution of lipid molecules in relation to water and ethanol molecules. With implications for chemistry, biology, and materials science, these insights into the intermolecular distances between solvent and lipid molecules are crucial for comprehending the dynamics and solvation behaviors of molecular systems in aqueous ethanol environments.

4. CONCLUSION

We assessed the stability of lipid nanoparticles (LNPs) and the impact of ethanol on their self-assembly using molecular dynamics (MD) simulations. We successfully created well-encapsulated LNP structures with varying N/P ratios by force field parameterization and MD simulations, optimizing the lipid-to-siRNA ratio to achieve total encapsulation. Understanding the dynamic interactions between lipid and siRNA components within LNPs is essential for comprehending their physicochemical features, as demonstrated by the measurement of N/P ratios. The influence of ethanol on LNP stability was clarified by further simulations conducted in an aqueous ethanol environment, which showed notable modifications in solvent accessibility and structure dynamics. The lipid components in the self-assembly system were found to be more stable when compared to aqueous ethanol, according to RMSD analysis. This suggests that ethanol might have induced some structural alterations. Furthermore, SASA analysis showed that ethanol increased the exposure of siRNA to solvent molecules, suggesting LNP degradation, by adding it to the mixture. Further evidence for ethanol infiltration into LNPs was provided by radial distribution function (RDF) and electron density profile (EDP) analysis. Taken together, our findings clarify how ethanol affects LNP stability and the kinetics of LNP self-assembly. The implications of these results for the development and refinement of LNPs for many biological applications, including medication delivery and gene therapy, are substantial.

Refrences

1) Bedrov, D., Piquemal, J. P., Borodin, O., MacKerell Jr, A. D., Roux, B., & Schröder, C. (2019). Molecular dynamics simulations of ionic liquids and electrolytes using polarizable force fields. Chemical reviews, 119(13), 7940-7995.

2) Bittner, J. P., Zhang, N., Huang, L., de María, P. D., Jakobtorweihen, S., & Kara, S. (2022). Impact of deep eutectic solvents (DESs) and individual DES components on alcohol dehydrogenase catalysis: connecting experimental data and molecular dynamics simulations. Green chemistry, 24(3), 1120-1131.

3) Castillo-Borja, F., & Bravo-Sánchez, U. I. (2021). Molecular dynamics simulation study of the performance of different inhibitors for methane hydrate growth. Journal of Molecular Liquids, 337, 116510.

4) Chaouiki, A., Lgaz, H., Zehra, S., Salghi, R., Chung, I. M., El Aoufir, Y., ... & Oudda, H. (2019). Exploring deep insights into the interaction mechanism of a quinazoline derivative with mild steel in HCl: electrochemical, DFT, and molecular dynamic simulation studies. Journal of Adhesion Science and Technology, 33(9), 921-944.

5) Figueiredo, N. M., Voroshylova, I. V., Koverga, V. A., Ferreira, E. S., & Cordeiro, M. N. D. (2019). Influence of alcohols on the inter-ion interactions in ionic liquids: A molecular dynamics study. Journal of Molecular Liquids, 294, 111538.

6) Li, G., Zheng, F., Huang, Q., Wang, J., Niu, B., Zhang, Y., & Long, D. (2022). Molecular insight into pyrolysis processes via reactive force field molecular dynamics: A state-of-the-art review. Journal of Analytical and Applied Pyrolysis, 166, 105620.

7) Liu, P., Liu, J., & Wang, M. (2019). Adsorption of ethanol molecules on the Al (1 1 1) surface: a molecular dynamic study. Royal Society open science, 6(1), 181189.

8) Lu, Q., Chen, F., Xiao, L., Yang, J., Hu, Y., Zhang, G., ... & Hao, G. (2022). Advances in the molecular simulation and numerical calculations of the green high-energy oxidant ADN. Materials Today Communications, 31, 103699.

9) Ma, Y., & Chew, J. W. (2022). Investigation of membrane fouling phenomenon using molecular dynamics simulations: A review. Journal of Membrane Science, 661, 120874.

10) Mandal, S., Zamindar, S., Sarkar, S., Murmu, M., Guo, L., Kaya, S., ... & Banerjee, P. (2023). Quantum chemical and molecular dynamics simulation approach to investigate adsorption behaviour of organic azo dyes on TiO2 and ZnO surfaces. Journal of Adhesion Science and Technology, 37(10), 1649-1665.

11) Mousavi, S. Z., Shadman, H. R., Habibi, M., Didandeh, M., Nikzad, A., Golmohammadi, M., ... & Razmjou, A. (2023). Elucidating the sorption mechanisms of environmental pollutants using molecular simulation. Industrial & Engineering Chemistry Research, 62(8), 3373-3393.

12) Pothoczki, S., Pusztai, L., & Bakó, I. (2019). Molecular dynamics simulation studies of the temperature-dependent structure and dynamics of isopropanol–water liquid mixtures at low alcohol content. The Journal of Physical Chemistry B, 123(35), 7599-7610.

13) R. Luginbuhl, B., Raval, P., Pawlak, T., Du, Z., Wang, T., Kupgan, G., ... & Reddy, G. M. (2022). Resolving atomic-scale interactions in nonfullerene acceptor organic solar cells with solid-state NMR spectroscopy, crystallographic modelling, and molecular dynamics simulations. Advanced Materials, 34(6), 2105943.

14) Róg, T., Girych, M., & Bunker, A. (2021). Mechanistic understanding from molecular dynamics in pharmaceutical research 2: lipid membrane in drug design. Pharmaceuticals, 14(10), 1062.

15) Svechkarev, D., Kyrychenko, A., Payne, W. M., & Mohs, A. M. (2018). Probing the self-assembly dynamics and internal structure of amphiphilic hyaluronic acid conjugates by fluorescence spectroscopy and molecular dynamics simulations. Soft Matter, 14(23), 4762-4771.

16) Wu, J., Gao, T., Guo, H., Zhao, L., Lv, S., Lv, J., ... & Ma, F. (2023). Application of molecular dynamics simulation for exploring the roles of plant biomolecules in promoting environmental health. Science of The Total Environment, 869, 161871.

17) Xia, Y., Zhang, R., Cao, Y., Xing, Y., & Gui, X. (2020). Role of molecular simulation in understanding the mechanism of low-rank coal flotation: A review. Fuel, 262, 116535.

18) Yao, X., Liu, Y., Li, T., Zhang, T., Li, H., Wang, W., ... & Yao, Z. (2020). Adsorption behavior of multicomponent volatile organic compounds on a citric acid residue waste-based activated carbon: Experiment and molecular simulation. Journal of hazardous materials, 392, 122323.

19) Zhang, P., Wu, H., Song, X., Liu, Y., & Cheng, X. (2022). Fuel molecular structure influences the polycyclic aromatic hydrocarbons formation of butanol/butane isomers: A ReaxFF molecular dynamics study. Fuel, 310, 122460.

20) Zheng, F., Ren, Z., Xu, B., Wan, K., Cai, J., Yang, J., ... & Long, D. (2021). Elucidating multiple-scale reaction behaviors of phenolic resin pyrolysis via TG-FTIR and ReaxFF molecular dynamics simulations. Journal of Analytical and Applied Pyrolysis, 157, 105222.

21) Mandal S, Vishvakarma P. Nanoemulgel: A Smarter Topical Lipidic Emulsion-based Nanocarrier. Indian J of Pharmaceutical Education and Research. 2023;57(3s):s481-s498.

22) Mandal S, Jaiswal DV, Shiva K. A review on marketed Carica papaya leaf extract (CPLE) supplements for the treatment of dengue fever with thrombocytopenia and its drawback. International Journal of Pharmaceutical Research. 2020 Jul;12(3).

23) Bhandari S, Chauhan B, Gupta N, et al. Translational Implications of Neuronal Dopamine D3 Receptors for Preclinical Research and Cns Disorders. African J Biol Sci (South Africa). 2024;6(8):128-140. doi:10.33472/AFJBS.6.8.2024.128-140

24) Tripathi A, Gupta N, Chauhan B, et al. Investigation of the structural and functional properties of starch-g-poly (acrylic acid) hydrogels reinforced with cellulose nanofibers for cu2+ ion adsorption. African J Biol Sci (South Africa). 2024;6(8): 144-153, doi:10.33472/AFJBS.6.8.2024.141-153

25) Mandal S, Bhumika K, Kumar M, Hak J, Vishvakarma P, Sharma UK. A Novel Approach on Micro Sponges Drug Delivery System: Method of Preparations, Application, and its Future Prospective. Indian J of Pharmaceutical Education and Research. 2024;58(1):45-63.

26) Mishra, N., Alagusundaram, M., Sinha, A., Jain, A. V., Kenia, H., Mandal, S., & Sharma, M. (2024). Analytical Method, Development and Validation for Evaluating Repaglinide Efficacy in Type Ii Diabetes Mellitus Management: a Pharmaceutical Perspective. Community Practitioner, 21(2), 29–37. https://doi.org/10.5281/zenodo.10642768

27) Singh, M., Aparna, T. N., Vasanthi, S., Mandal, S., Nemade, L. S., Bali, S., & Kar, N. R. (2024). Enhancement and Evaluation of Soursop (Annona Muricata L.) Leaf Extract in Nanoemulgel: a Comprehensive Study Investigating Its Optimized Formulation and Anti-Acne Potential Against Propionibacterium Acnes, Staphylococcus Aureus, and Staphylococcus Epidermidis Bacteria. Community Practitioner, 21(1), 102–115. https://doi.org/10.5281/zenodo.10570746

28) Khalilullah, H., Balan, P., Jain, A. V., & Mandal, S. (n.d.). Eupatorium Rebaudianum Bertoni (Stevia): Investigating Its Anti-Inflammatory Potential Via Cyclooxygenase and Lipooxygenase Enzyme Inhibition - A Comprehensive Molecular Docking And ADMET. Community Practitioner, 21(03), 118–128. https://doi.org/10.5281/zenodo.10811642

29) Mandal, S. Vishvakarma, P. Pande M.S., Gentamicin Sulphate Based Ophthalmic Nanoemulgel: Formulation and Evaluation, Unravelling A Paradigm Shift in Novel Pharmaceutical Delivery Systems. Community Practitioner, 21(03), 173-211. https://doi.org/10.5281/zenodo.10811540

30) Mandal, S., Tyagi, P., Jain, A. V., & Yadav, P. (n.d.). Advanced Formulation and Comprehensive Pharmacological Evaluation of a Novel Topical Drug Delivery System for the Management and Therapeutic Intervention of Tinea Cruris (Jock Itch). Journal of Nursing, 71(03). https://doi.org/10.5281/zenodo.10811676

31) Mishra, N., Alagusundaram, M., Sinha, A., Jain, A. V., Kenia, H., Mandal, S., & Sharma, M. (2024). Analytical Method, Development and Validation for Evaluating Repaglinide Efficacy in Type Ii Diabetes Mellitus Management: a Pharmaceutical Perspective. Community Practitioner, 21(2), 29–37. https://doi.org/10.5281/zenodo.10642768

32) Singh, M., Aparna, T. N., Vasanthi, S., Mandal, S., Nemade, L. S., Bali, S., & Kar, N. R. (2024). Enhancement and Evaluation of Soursop (Annona Muricata L.) Leaf Extract in Nanoemulgel: a Comprehensive Study Investigating Its Optimized Formulation and Anti-Acne Potential Against Propionibacterium Acnes, Staphylococcus Aureus, and Staphylococcus Epidermidis Bacteria. Community Practitioner, 21(1), 102–115. https://doi.org/10.5281/zenodo.10570746

33) Gupta, N., Negi, P., Joshi, N., Gadipelli, P., Bhumika, K., Aijaz, M., Singhal, P. K., Shami, M., Gupta, A., & Mandal, S. (2024). Assessment of Immunomodulatory Activity in Swiss Albino Rats Utilizing a Poly-Herbal Formulation: A Comprehensive Study on Immunological Response Modulation. Community Practitioner, 21(3), 553–571. https://doi.org/10.5281/zenodo.10963801

34) Mandal S, Vishvakarma P, Bhumika K. Developments in Emerging Topical Drug Delivery Systems for Ocular Disorders. Curr Drug Res Rev. 2023 Dec 29. doi: 10.2174/0125899775266634231213044704. Epub ahead of print. PMID: 38158868.

35) Abdul Rasheed. A. R, K. Sowmiya, S. N., & Suraj Mandal, Surya Pratap Singh, Habibullah Khallullah, N. P. and D. K. E. (2024). In Silico Docking Analysis of Phytochemical Constituents from Traditional Medicinal Plants: Unveiling Potential Anxiolytic Activity Against Gaba, Community Practitioner, 21(04), 1322–1337. https://doi.org/10.5281/zenodo.11076471

36) Pal N, Mandal S, Shiva K, Kumar B. Pharmacognostical, Phytochemical and Pharmacological Evaluation of Mallotus philippensis. Journal of Drug Delivery and Therapeutics. 2022 Sep 20;12(5):175-81.

37) Singh A, Mandal S. Ajwain (Trachyspermum ammi Linn): A review on Tremendous Herbal Plant with Various Pharmacological Activity. International Journal of Recent Advances in Multidisciplinary Topics. 2021 Jun 9;2(6):36-8.

38) Mandal S, Jaiswal V, Sagar MK, Kumar S. Formulation and evaluation of carica papaya nanoemulsion for treatment of dengue and thrombocytopenia. Plant Arch. 2021;21:1345-54.

39) Mandal S, Shiva K, Kumar KP, Goel S, Patel RK, Sharma S, Chaudhary R, Bhati A, Pal N, Dixit AK. Ocular drug delivery system (ODDS): Exploration the challenges and approaches to improve ODDS. Journal of Pharmaceutical and Biological Sciences. 2021 Jul 1;9(2):88-94.

40) Shiva K, Mandal S, Kumar S. Formulation and evaluation of topical antifungal gel of fluconazole using aloe vera gel. Int J Sci Res Develop. 2021;1:187-93.

41) Ali S, Farooqui NA, Ahmad S, Salman M, Mandal S. Catharanthus roseus (sadabahar): a brief study on medicinal plant having different pharmacological activities. Plant Archives. 2021;21(2):556-9.

42) Mandal S, Vishvakarma P, Verma M, Alam MS, Agrawal A, Mishra A. Solanum Nigrum Linn: An Analysis Of The Medicinal Properties Of The Plant. Journal of Pharmaceutical Negative Results. 2023 Jan 1:1595-600.

43) Vishvakarma P, Mandal S, Pandey J, Bhatt AK, Banerjee VB, Gupta JK. An Analysis Of The Most Recent Trends In Flavoring Herbal Medicines In Today's Market. Journal of Pharmaceutical Negative Results. 2022 Dec 31:9189-98.

44) Mandal S, Vishvakarma P, Mandal S. Future Aspects And Applications Of Nanoemulgel Formulation For Topical Lipophilic Drug Delivery. European Journal of Molecular & Clinical Medicine.;10(01):2023.

45) Chawla A, Mandal S, Vishvakarma P, Nile NP, Lokhande VN, Kakad VK, Chawla A. Ultra-Performance Liquid Chromatography (Uplc).

46) Mandal S, Raju D, Namdeo P, Patel A, Bhatt AK, Gupta JK, Haneef M, Vishvakarma P, Sharma UK. Development, characterization, and evaluation of rosa alba l extract-loaded phytosomes.

47) Mandal S, Goel S, Saxena M, Gupta P, Kumari J, Kumar P, Kumar M, Kumar R, Shiva K. Screening of catharanthus roseus stem extract for anti-ulcer potential in wistar rat.

48) Shiva K, Kaushik A, Irshad M, Sharma G, Mandal S. Evaluation and preparation: herbal gel containing thuja occidentalis and curcuma longa extracts.

49) Vishvakarma P, Kumari R, Vanmathi SM, Korni RD, Bhattacharya V, Jesudasan RE, Mandal S. Oral Delivery of Peptide and Protein Therapeutics: Challenges And Strategies. Journal of Experimental Zoology India. 2023 Jul 1;26(2).